

SPE 18089

Prediction of Xanthan Rheology in Porous Media

by W.J. Cannella, C. Huh, and R.S. Seright,* Exxon Production Research Co.

SPE Members

*Currently with New Mexico Petroleum Research Center

Copyright 1988, Society of Petroleum Engineers

This paper was prepared for presentation at the 63rd Annual Technical Conference and Exhibition of the Society of Petroleum Engineers held in Houston, TX, October 2-5, 1988.

This paper was selected for presentation by an SPE Program Committee following review of information contained in an abstract submitted by the author(s). Contents of the paper, as presented, have not been reviewed by the Society of Petroleum Engineers and are subject to correction by the author(s). The material, as presented, does not necessarily reflect any position of the Society of Petroleum Engineers, its officers, or members. Papers presented at SPE meetings are subject to publication review by Editorial Committees of the Society of Petroleum Engineers. Permission to copy is restricted to an abstract of not more than 300 words. Illustrations may not be copied. The abstract should contain conspicuous acknowledgment of where and by whom the paper is presented. Write Publications Manager, SPE, P.O. Box 833836, Richardson, TX 75083-3836. Telex, 730989 SPEDAL.

Γ

ABSTRACT

The flow behavior of xanthan in porous media has been investigated experimentally, and also theoretically using effective medium theory. In the experimental portion of this study, the rheology of a commercially-available xanthan broth was characterized in porous media and viscometers and compared for a wide range of polymer concentrations (300 to 1600 ppm), effective brine permeabilities (40 to 800 md), residual oil saturations (0 to 29%), temperatures (25° and 80°C), and rock lithologies (sandstones and carbonates). An apparent shear rate equation having no adjustable parameters was developed and proved to be effective in relating the flow behavior of a given polymer solution in porous media at one set of conditions to the behavior at all other porous media conditions tested as well as to the rheology in a viscometer. Although the shear rate dependence on flow velocity (first order) and effective permeability (negative one-half order) agrees with that predicted by traditional capillary bundle model approaches, the value of the experimentally determined constant coefficient is larger than those predicted by the models.

The basis for the shear rate equation employed above has been studied theoretically with the assumption that the xanthan solution rheologies approximately follow the power-law relation. The apparent viscosity for a power-law fluid flowing in a porous medium is derived employing the effective medium approximation of percolation theory. In this approach, a porous medium is modeled as a network of capillary tubes, in which the radii of tubes are randomly distributed using a prescribed probability distribution. The apparent viscosity expression obtained is similar to that from the capillary bundle model, but the coefficient values are different, as observed experimentally. This difference is a consequence of the connectivity of flow channels and their variable cross-section. Due to its shear-thinning nature, a

power-law fluid flows mainly through the wide channels of porous media, and largely bypasses small-scale pore channels of the porous body. The capillary bundle model cannot describe this tendency of a shear-thinning fluid.

I. INTRODUCTION

Process models developed to predict production characteristics of enhanced oil recovery projects using polymers for mobility control require information about the rheological behavior of the polymer solution in porous media. One method to obtain this information involves performing time-consuming core-flood studies using the polymer solution and reservoir core material at each specific reservoir condition of interest, such as permeability, porosity, and fluid saturations. Development of an equation that can be used to predict the flow behavior in porous media from easy-to-obtain viscometer data and/or extend the results from one coreflood to other conditions is highly desirable.

An equation relating rheology in viscometers to flow behavior in porous media is most suitable for pseudoplastic ("shear-thinning") fluids. A correlation is not needed for Newtonian fluids since the viscosity is independent of shear rate, while the viscoelastic behavior exhibited by many synthetic polymers is not observed in conventional viscometers. Xanthan biopolymer is one excellent candidate for such a correlation because it is almost purely pseudoplastic ("shear thinning") with negligible elastic effects. Interest in the use of this polymer for oil recovery operations has been high due to favorable properties which include: (1) good injectivity resulting from pseudoplasticity, (2) relative insensitivity of viscosity to salinity, and (3) excellent resistance to shear degradation over the shear rate range of interest in typical oilfield applications.

References and illustrations at end of paper.

The flow behavior of xanthan solutions in both viscometers and consolidated porous media has been previously studied by other investigators including Teeuw and Hesselink,¹ Willhite and Uhl,² and Chauveteau³. In these studies, the flow in porous media was compared to viscometer data by calculating apparent viscosities from Darcy's law and converting flow rates into "effective" shear rates using the following equation:

$$\dot{\gamma}_{\text{eff}} = C \left(\frac{3n+1}{4n} \right) \frac{u}{\sqrt{k\phi}} \quad [1]$$

In this equation, which is derived from the capillary bundle model for flow of non-Newtonian fluids, u is the Darcy velocity, k is permeability, and ϕ is porosity. The value of n is related to the local slope of the log-log plot of viscosity vs. shear rate (or velocity) at the shear rate (velocity) of interest. The theoretical value of C depends on the approach taken and the values used to account for the tortuosity of the porous medium. Detailed discussions of the different derivations can be found in Refs. 1 and 4.

Teeuw and Hesselink¹ compared the flow behavior of xanthan solutions in the power-law regime in Bentheim sandstone and a viscometer. They reported that the power-law exponents in the viscometer and porous media were essentially equal within experimental error. However, the apparent shear rates in porous media were underestimated when the values of C derived from several different approaches of capillary bundle theory were used. It is not apparent within experimental error whether a single value of C can align their porous media shear rates with those of the viscometer for all solutions and permeabilities tested.

In contrast to Teeuw and Hesselink's results, Willhite and coworkers^{2,5} reported that the measured power-law exponents for flow of xanthan solutions in Berea sandstone cores and Ottawa sandpicks were lower than the values obtained in a viscometer. Thus, empirical equations had to be developed to relate the flow of each solution in porous media to viscometer data. In flow tests of dilute xanthan solutions in 3.3 to 256 md Fontainebleau sandstones, Chauveteau^{3,6} recently postulated that hydrodynamic exclusion of xanthan molecules from the vicinity of pore walls was responsible for the lower apparent viscosities he observed in porous media relative to viscometer values in the first Newtonian regime.

Based on the results of these previous studies, the viability of predicting the flow behavior in porous media is uncertain.

The results obtained in the present study of xanthan solution flow behavior in consolidated porous media and viscometers demonstrate that an equation similar to eq. [1] with a single value of C determined from the study can be used to relate the flow behavior in porous media having different permeabilities (40 to 800 md), oil saturations (zero and residual oil saturation), and lithologies (sandstones and carbonates). In addition, the flow of solutions prepared from the xanthan broth tested in this study can be predicted from viscometer data obtained for the polymer concentrations (300 to 1600 ppm) and temperatures (25 and 80°C) studied. The experimental results are presented in Section II.

In view of the simplistic nature of the capillary bundle model in representing porous media, an intriguing question to ask is why the equation could so successfully correlate the apparent viscosity of xanthan solutions in porous media. We show in Section III that, even when a more realistic model of porous media with a network of capillary tubes is employed, the functional form of eq. [1] is approximately correct; and that the connectivity of flow channels and their variable cross-section could explain why the value of C is higher than the values predicted from the capillary bundle model approaches. Specifically, a model of a porous medium, in which capillary tubes of varying radii are interconnected, is employed and the flow of a power-law fluid in such a network is considered. The apparent viscosity expression is then derived by applying the so-called effective medium theory. In particular, the apparent viscosity of polymer is considered in a network having a bimodal distribution of tube radii, with examples of two simplest cases: (i) a bundle of unconnected capillary tubes, with each tube having stepwise changes in radius along its length, causing a series of constrictions and expansions; and (ii) a network of capillary tubes of a uniform radius, in which a certain fraction of the connections are blocked randomly, thus creating interconnected, tortuous passages. Conclusions are given in Section IV.

II. EXPERIMENTAL INVESTIGATION

II.1. PROCEDURES

The flow behavior of 1200 ppm xanthan solution was investigated in Berea sandstone and carbonate cores at 25°C both in the presence and absence of residual oil. The effective permeabilities ranged from 40 to 800 md. The rheologies of 300, 600, and 1600 ppm xanthan solutions were also studied in nominal 800 md Berea sandstone. Limited studies were also conducted at 80°C.

Polymer solutions were prepared by diluting a commercially available xanthan broth with filtered (0.22 micron filter) synthetic 3.3% brine (3% NaCl, 0.3% CaCl₂). The dilute solutions were mixed with a homogenizer for 3 min/l at a variac setting of 120V. The solutions were typically filtered through a Millipore AP-15 prefilter, although in some cases the more extensive filtration technique recommended by Chauveteau and Kohler⁷ was used. Formaldehyde was added to the solutions tested at 25°C. A vacuum pump was used to degas the solutions prior to the viscometer and coreflood experiments. An oxygen scavenger, Na₂S₂O₄, was added to the degassed solution tested at 80°C to prevent loss of viscosity due to thermal-oxidative degradation. Polymer concentrations were determined by high-performance liquid chromatography (HPLC) analysis.

Viscosities were measured at 25°C with a Contraves LS-30 viscometer. A capillary viscometer was used under anaerobic conditions at 80°C. Corefloods were conducted with Berea sandstone and carbonate cores. The cores were initially evacuated and then saturated with degassed brine. For some cores, a residual oil saturation was established by displacing the brine with dodecane and subsequently waterflooding to residual oil. The waterflood to displace oil was conducted at pressure gradients at least two times higher than the maximum gradient established

during the polymer experiments. Brine permeabilities were determined at several flow rates.

During both brine and polymer injection, pressure drops were measured across several core segments using diaphragm type pressure transducers. The excellent agreement of pressure drop in all core segments indicated that anomalous behavior such as entrance or exit effects were insignificant. Apparent viscosities were determined at each velocity using Darcy's law:

$$\mu_{app} = \frac{k\Delta P}{uL} \quad [2]$$

II.2. VISCOSITY RESULTS

The viscometer rheograms for the 300 to 1600 ppm xanthan solutions are presented in Fig. 1. Over the range of shear rates investigated, the solutions exhibited Newtonian behavior at very low shear rates and power-law pseudoplastic behavior at moderate-to-high shear rates. At shear rates higher than those shown in Fig. 1, the solutions would exhibit a second Newtonian regime. Thus, over the entire shear rate range, the viscometer rheology can adequately be fit with a Carreau expression²⁵:

$$\mu = \mu_{\infty} + (\mu_0 - \mu_{\infty}) \left[1 + \left(\frac{K}{\mu_0} \right)^{\frac{2}{n-1}} \dot{\gamma}^2 \right]^{\frac{n-1}{2}} \quad [3]$$

where μ_0 represents the Newtonian viscosity at zero shear rate, μ_{∞} represents the Newtonian viscosity at infinite shear rate, K represents the consistency index, and n represents the power-law exponent.

At moderate to high shear rates for $\mu_0 \gg \mu_{\infty}$, eq. [3] reduces to the power-law expression:

$$\mu = K \dot{\gamma}^{n-1} \quad [4]$$

Values for μ_0 , K , and n , determined from the viscometer rheograms, are reported in Table I for each concentration. The value of μ_{∞} is assumed to be equal to the brine viscosity value of 1.0 cp for all concentrations.

II.3. POROUS MEDIA RESULTS

II.3.1. BASE CASE

The apparent viscosity versus Darcy velocity ($u = Q/A$) curve for the flow of 1200 ppm solution in 264 md Berea sandstone is illustrated in Fig. 2. Over most of the velocity range investigated, the log-log plot is linear, suggesting that μ_{app} is proportional to u^{n-1} . The value of n that is obtained from the slope of the linear portion of the curve is 0.49. This value is essentially identical to the 0.48 value obtained from the viscometer results.

To compare the porous media and viscometer data, the flow velocities in porous media were converted to apparent shear rates using the following equation:

$$\dot{\gamma}_{app} = C \left(\frac{3n+1}{4n} \right)^{\frac{n}{n-1}} \frac{u}{\sqrt{k\phi}} \quad [5]$$

where the units are $\dot{\gamma}_{app} = \text{sec}^{-1}$, $u = \text{cm/sec}$, and $k = \text{cm}^2$. The derivation of this equation is discussed in Appendix A.

The apparent viscosities obtained in porous media are compared with the viscometer measured values in Fig. 3. In the power-law regime, the alignment of both data sets was effected by using a value of $C = 6.0$. This value is higher than the values predicted by the capillary bundle model derivations^{1,4,13,14} which are summarized in Table II. The higher value of C determined experimentally is consistent with the trend predicted by effective medium theory, as discussed later in Section III of this study.

At low shear rates, the solution continues to exhibit power-law behavior in porous media while Newtonian behavior is obtained in the viscometer. Thus, the apparent viscosities predicted from the viscometer data are lower than the values obtained in the porous media. At high velocities, the flow becomes less pseudoplastic and the apparent viscosity approaches a Newtonian value of μ_{∞} at infinite shear rate. Over the entire velocity range investigated, the porous media data appears to fit a modified power-law expression of the form:

$$\mu_{app} = \mu_{\infty} + K \dot{\gamma}_{app}^{n-1} = \mu_{\infty} + K \left(\frac{3n+1}{4n} \right)^n \left(\frac{6.0u}{\sqrt{k\phi}} \right)^{n-1} \quad [6]$$

The solid line in Fig. 3 represents the apparent viscosities predicted by eq. [6] using the viscometer measured values for K and n from Table I and $\mu_{\infty} = 1.0$. Excellent agreement is obtained between the predicted and actual values. As shown in the next sub-section, this equation also proves to be valid for different permeabilities, lithologies (sandstones and carbonates), and residual oil saturations.

The transition from the first Newtonian regime to pseudoplastic behavior in viscometers is typically attributed to the onset of alignment of polymer molecules with the flow field and decreased interactions (e.g. entanglements) between polymer molecules. At very low flow rates, the rod-like xanthan molecules are not likely to be aligned with the flow field. In porous media where the flow channel dimensions approach those of the polymer molecules, the nonalignment at low flow rates as well as interaction with neighboring molecules in concentrated solutions may cause additional resistance to flow as polymer molecules pass through flow constrictions. This could be responsible for the observed power-law behavior for these solutions at low shear rates in porous media. Results presented later illustrate that Newtonian behavior can be obtained at low shear rates in porous media at dilute concentrations where intermolecular interactions are expected to be minimal.

An additional resistance to flow could also be obtained if microgels were present in solution or if polymer retention continuously reduced the effective permeability of the porous medium. Neither of these phenomena are believed to have been significant in this study. Excellent agreement was obtained for the apparent viscosities in the inlet, middle, and outlet core segments, as deduced from the pressure measurements. If polymer aggregates were present, the apparent viscosity in the inlet segment would be

expected to increase with time at low flow rates due to continuous trapping of aggregates. Large polymer aggregates were likely not present because the polymer solutions were prepared from broths. Data obtained by Kolodziej⁶ and Kohler and Chauveteau⁹ suggest that microgels are much less likely to be present in solutions prepared from broths than those prepared from powders. In addition, in the present study, pseudoplastic behavior was also observed at very low flow rates for one solution that was prepared using the slow-filtration technique developed by Chauveteau and Kohler⁷ to remove microgels from solution. Residual resistance factor measurements also indicated little or no change in core permeability as a result of polymer injection.

II.3.2. INFLUENCE OF SOLUTION AND RESERVOIR PROPERTIES

The applicability of the conclusions obtained in the base case was studied further by investigating the effects of polymer concentration, permeability, lithology, temperature, and residual oil. The results of these studies are summarized below.

Rock Permeability and Lithology

The flow behavior of 1200 ppm xanthan solution was further studied in oil-free Berea sandstone cores having permeabilities of 100 and 740 md. The applicability of eqs. [5] and [6] with $C = 6.0$ for these permeability levels is demonstrated in Fig. 4. The data for all permeabilities tested can be fit with a single curve. In addition, excellent agreement is obtained between the porous media data and the values predicted from viscometer data using eq. [6].

The effects of lithology were also investigated by characterizing the flow behavior of 1200 ppm solution in carbonate cores. The permeabilities of these cores ranged from 47 to 440 md. Fig. 5 indicates that eq. [5] with a value of $C = 6.0$ effectively represents the shear rate in these cores. Thus, the value of C appears to be independent of permeability and lithology, at least for the range of cores and solutions tested in this study.

It is important to note that in all of these tests, permeabilities were not significantly reduced as a result of polymer injection. This was confirmed by residual resistance factor measurements that did not exceed a value of 1.1. Eq. [6] would not be expected to apply for cores in which the permeability was significantly reduced due to polymer retention.

Residual Oil

In oilfield applications the effective aqueous-phase permeability is typically lower than the absolute permeability of the porous medium due to the presence of residual or flowing oil. For these situations, it is likely that eq. [5] must be modified to reflect the effective aqueous permeability and saturation. An equation of the following form is proposed as an extension of eq. [5]:

$$\dot{\gamma}_{app} = 6.0 \left(\frac{3n+1}{4n} \right)^{\frac{n}{n-1}} \frac{u}{\sqrt{k_{aq} S_{aq} \phi}} \quad [7]$$

where k_{aq} and S_{aq} represent the effective aqueous permeability and fractional saturation at residual

oil, respectively. Equation [5] is a specific case of this equation for $S_{aq} = 1$ (i.e., oil-free cores).

To test this equation, the flow behavior of 1200 ppm xanthan was studied in Berea sandstone cores having a residual oil saturation. The results for two cores having effective brine permeabilities of 260 md and 52 md at residual oil are presented in Fig. 6. Also included in the plot are the results obtained from the oil-free core having a permeability of 264 md. The solid curve represents the apparent viscosities predicted from the viscometer data and eq. [8] below:

$$\mu_{app} = \mu_{\infty} + K \left(\frac{3n+1}{4n} \right)^n \left(\frac{6.0u}{\sqrt{k_{aq} S_{aq} \phi}} \right)^{n-1} \quad [8]$$

The excellent agreement between the predicted and experimental values indicates that eq. [8] can be used to effectively represent the flow behavior in the porous media tested both in the absence and presence of residual oil.

The complete data set obtained for all of the tests with the 1200 ppm solution at 25°C is presented in Fig. 7. The flow behavior in any of the cores tested can be predicted from the results obtained in any one of the cores or from the viscosity data using eqs. [7] and [8].

Polymer Concentration

To establish the effects of polymer concentration on flow behavior, the flow of 300, 600, and 1600 ppm xanthan solutions was studied in 765 md Berea sandstone core. The apparent viscosities in porous media are plotted in Fig. 8, along with the viscometer values. Porous media shear rates were calculated from eq. [5] using the value of $C = 6.0$ that was determined from the test with 1200 ppm solution. The excellent agreement that is obtained in the power-law region between the porous media and viscometer values for all concentrations suggests that eq. [5] is valid and that the value of C is independent of polymer concentration.

For concentrations of 600 ppm and higher, power-law behavior was also exhibited in porous media at very low shear rates. The solid lines in Fig. 8 for these solutions represent the apparent viscosities predicted by eq. [6]. The apparent viscosities predicted from eq. [6] agree very well with the measured values.

In contrast to the results obtained at low shear rates for high concentrations, Newtonian behavior was observed in porous media for the 300 ppm solution. This concentration is believed to be close in value to the overlap concentration for this solution, C^* , below which interactions between polymer molecules are negligible. As noted earlier, the observed power-law behavior for more concentrated solutions at low shear rates may reflect an increased resistance to flow due to molecular interactions in the pore spaces. Additional testing is needed to verify this hypothesis.

For the 300 ppm solution, and presumably for lower concentration solutions, the extended power-law behavior predicted by eq. [6] is not applicable. For

these solutions, the Carreau expression of eq. [3] is suitable. The agreement between the porous media and viscometer viscosities for the 300 ppm solution in Fig. 8 suggests that the values for μ_0 , μ_∞ , K , and n can be determined from the viscometer and used to predict the flow behavior in porous media. The solid curve for this solution in Fig. 8 represents the apparent viscosities predicted by eq. [3] using $\mu_0 = 8.6$ cp, $\mu_\infty = 1.0$ cp, $K = 17$ cp-sec $^{n-1}$ and $n = 0.75$.

Temperature

The impact of elevated temperature on the flow behavior was investigated for the 1200 ppm solution at 80°C. The viscometer and porous media results are presented in Fig. 9. In contrast to the 25°C results, Newtonian behavior is observed for this concentration at 80°C in porous media at low apparent shear rates. Apparent viscosities in porous media agree with viscometer results over the entire apparent shear rate range tested and the Carreau expression, eq. [3], applies. The solid curve in Fig. 9 represents the apparent viscosities predicted by eq. [3] using $\mu_0 = 8.8$ cp, $\mu_\infty = 0.35$ cp, $K = 30$ cp sec $^{n-1}$, and $n = 0.65$.

Differences in the structural or flexibility characteristics of the xanthan molecules and/or degree of intermolecular interactions may be responsible for the difference in flow behavior obtained at 25°C and elevated temperature. It has been reported^{10,24} that xanthan can undergo an "order-disorder" (helix-coil) transition and/or denaturation. These conformational changes are influenced by temperature, the salinity and hardness of the solution, and possibly the characteristics of the specific xanthan tested. Additional testing is needed to understand the changes and their impact on flow behavior.

II.4. COMPARISON WITH PREVIOUS STUDIES

For the solutions tested in this study, the flow behavior in porous media under a wide variety of conditions can essentially be predicted from one set of coreflood results or from viscometer data by using eq. [7] to calculate the apparent shear rate in porous media. This equation also appears to be applicable to some, but not all, of the results reported in the literature.

As discussed earlier, Teeuw and Hesselink¹ reported that the power-law exponents obtained in viscometer and coreflood tests of xanthan solutions in Bentheim sandstone were similar. However, as shown in Fig. 10(a), consistency indices calculated from the porous media data, K_{core} , $C = \sqrt{2}$, were lower than the values measured with the viscometer, K . These results indicate that the porous media shear rates were underestimated by using a value of $C = \sqrt{2}$. As illustrated in Fig. 10(b), the agreement between the porous media and viscometer values can be improved by using the value $C = 6.0$ obtained in the present study.

From studies of carboxymethylcellulose, Gogarty, et al.¹¹ reported that the rheograms of glass bead and sandpacks could be aligned with those obtained in a viscometer by using eq. [1] with the value of $C = 50/\sqrt{150}$. Shear rates calculated from eq. [5] with our value of $C = 6.0$ are identical to Gogarty's values for $n = 0.6$ and within experimental accuracy (less than 10% difference) for values of n between

0.45 and 0.85. Thus, the applicability of eqs. [5] and [7] appears to extend to Gogarty's data and thus beyond the flow of xanthan in consolidated porous media.

In contrast to the results of the present study, Willhite and Uhl² and Hejri et al.⁵ reported that the measured power-law exponents for flow of xanthan solutions in Berea sandstone cores and unconsolidated sandpacks were lower than viscometer values. Thus in those tests, flow behavior in porous media could not be predicted a priori from viscometer data.

At very low shear rates, the observed flow behavior in porous media in the present study also differs with results obtained by Chauveteau and co-workers.^{3,6} In the present study, power-law behavior was obtained at 25°C for solutions having concentrations of 600 ppm and higher. Newtonian behavior was exhibited by the 300 ppm solution at 25°C and the porous media apparent viscosity was equal to the viscometer-measured value. Chauveteau has also reported Newtonian behavior for flow of xanthan solutions in glass bead packs, sand packs, and sandstones at low shear rates. However, the apparent viscosities in porous media were lower than the values measured in a viscometer. As the permeability decreased, the apparent viscosity decreased. This was attributed to depletion layer effects in which polymer molecules are sterically hindered from the vicinity of pore walls. In the present study, the observed agreement between porous media and viscometer viscosities for a wide variety of conditions suggests that depletion layer effects are not significant for the solutions tested. The difference in the two studies may possibly be attributed to different polymer solution properties such as conformation and/or flexibility of the polymer molecules, solution concentration, and salinity. For the solutions used in the present study, the average molecular weight and the intrinsic viscosity values are consistent with the values reported by Holzwarth¹² for solutions of double-stranded xanthan. In contrast, the solutions used by Chauveteau consisted of single-stranded xanthan having an average molecular weight of 1.8×10^6 and intrinsic viscosity of 4300 cc/g. In addition, the solution concentration in Chauveteau's sandstone tests is believed to be significantly below the overlap concentration (C^*) whereas in the present study the concentrations were typically above C^* . Concentration differences may not be the complete answer, however, since Chauveteau's tests with higher concentration solutions in SiC packs suggest that depletion layer effects become more significant as concentration increases.

Additional tests are needed to fully understand the causes for the different results obtained by various investigators.

III. THEORETICAL DERIVATION

In this section, the flow behavior of a power-law fluid is studied theoretically by employing a more realistic model than traditional capillary bundle model approaches^{4,13,14}. As indicated in Section II, these approaches underestimate the value of the coefficient C in the shear rate expression. This is not surprising, as the capillary bundle model cannot describe the connectivity of flow channels and their variable cross-section. Typically, the "tortuosity factor"⁴ is arbitrarily included in the model

to account for the tortuous flow paths in the porous body. Employing a more realistic model of porous media that features the connectivity of flow channels and their variable cross-section has been difficult due to the accompanying mathematical complexity.

The model used in the present study remedies the above shortcomings. It consists of a regular network of capillary tubes, and the radii of tubes, which have a prescribed probability distribution, are randomly distributed in the network (see Fig. 11). Such a model has been employed by Koplik¹⁵ and Levine and Cuthiell¹⁶ to study the flow of Newtonian fluids in porous media. The average flow behavior in such a network then can be fairly accurately described by employing the so-called effective medium theory. The main objective of this theoretical analysis is to provide insight as to why the predicted apparent shear rate from the capillary bundle model is much lower than suggested by experimental data.

III.1. EFFECTIVE MEDIUM THEORY FOR FLOW IN POROUS MEDIA

The effective medium theory was originally developed to calculate the electrical conductivity for a regular network of resistors with randomly distributed conductivities^{17,18}. If g is the conductivity of a channel and $p(g)$ is the normalized probability distribution for g , the effective medium theory shows that the conductivity for all channels of the network can be replaced by a single, effective conductivity, g_m , which can be obtained from the equation:

$$\int_0^{\infty} \frac{(g_m - g) p(g) dg}{[g + (\frac{z}{2} - 1)g_m]} = 0 \quad [9]$$

where z is the coordination number for the network.

Consider now a regular network of capillary tubes, in which the tube radii of a given probability distribution are randomly placed in the network (Fig. 11). The coordination number (z) then represents the connectivity of a pore with its neighboring pores. If water without polymer flows in such a network, the flow rate in a tube of radius r is given by

$$q = \frac{\pi r^4}{8\mu_w} \left(\frac{\Delta P}{L} \right) \quad [10]$$

where μ_w is the viscosity of water. The flow conductivity for water in the tube can be defined as

$$g(r) = \frac{\pi r^4}{8\mu_w} \quad [11]$$

In this and the later derivation for a power-law fluid, the pressure drop which occurs at the tube joints, due to change of tube cross-section¹⁹ and change of flow direction, is neglected.

The effective flow conductivity for water in the network, g_m , can be obtained from eq. [9], in which $p(g)$ is now replaced by $p(r)$, the normalized pore size distribution. The average flow rate for the tubes of the network can now be given as:

$$q_m = \frac{\pi r_m^4}{8\mu_w} \left(\frac{\Delta P}{L} \right) \quad [12]$$

where r_m is the effective tube radius calculated from eq. [11] with $g = g_m$. The Darcy velocity of the network is then

$$u = \frac{\phi q_m}{\pi a^2} = \frac{\phi r_m^2}{8\mu_w \epsilon^2} \left(\frac{\Delta P}{L} \right) \quad [13]$$

where

$$\pi a^2 = \pi \int_0^{\infty} r^2 p(r) dr \quad [14]$$

is the average cross-sectional area of the tubes in the network, and we also define $\epsilon = a/r_m$. From the Darcy's equation and eq. [13], we obtain the permeability of the network as

$$k = \frac{\phi r_m^2}{8\epsilon^2} \quad [15]$$

III.2. NETWORK OF CAPILLARY TUBES WITH A POWER-LAW FLUID

Suppose now a polymer solution which follows the power-law viscosity equation [4] flows through the network. The relation between q and $(\Delta P/L)$ in a tube of radius r is given by

$$q = \frac{\pi r^{3+\frac{1}{n}}}{(3+\frac{1}{n})(2K)^{\frac{1}{n}}} \left(\frac{\Delta P}{L} \right)^{\frac{1}{n}} \quad [16]$$

The flow conductivity for the power-law fluid is now defined as

$$G = \frac{\pi r^{3+\frac{1}{n}}}{(3+\frac{1}{n})(2K)^{\frac{1}{n}}} \quad [17]$$

Because the effective medium theory is based on the linear relationship between the flux and the potential, a special manipulation is needed to apply the theory to the non-linear relation between flux and potential (pressure gradient) given by eq. [16]. The application of the effective medium theory for our particular situation is described in Appendix B. As given by eq. [B5], the pressure gradient for the tube with the conductivity of G can be expressed in terms of the average pressure gradient $(\Delta P/L)_m$, and the effective conductivity, G_m , as

$$\left(\frac{\Delta P}{L} \right) = \left[\frac{\frac{z}{2} G_m}{G + (\frac{z}{2} - 1)G_m} \right]^n \left(\frac{\Delta P}{L} \right)_m \quad [18]$$

According to the effective medium theory, the variations of the pressure gradient with respect to

the average value, $(\Delta P/L)_m$, should vanish when averaged over the whole network

$$\int_0^{\infty} \left[\left(\frac{\Delta P}{L} \right) - \left(\frac{\Delta P}{L} \right)_m \right] p(r) dr = 0 \quad [19]$$

from which follows the equivalent of eq. [9]:

$$\int_0^{\infty} \left[\left(\frac{\frac{z}{2} G_m}{G + (\frac{z}{2} - 1) G_m} \right)^n - 1 \right] p(r) dr = 0 \quad [20]$$

The relation between q and $(\Delta P/L)$ in the effective network will then be

$$q_m = G_m \left(\frac{\Delta P}{L} \right)^{\frac{1}{n}} \quad [21]$$

Larson²⁰ has shown, from volume averaging arguments, that the relation between flux and pressure gradient for a power-law fluid in porous media should take the form of [21].

The Darcy velocity for the network can now be given as

$$u = \frac{\phi q_m}{\pi a^2} = \frac{\phi (\lambda r_m)^3 + \frac{1}{n}}{(3 + \frac{1}{n}) (\epsilon r_m)^2 (2K)^{\frac{1}{n}}} \left(\frac{\Delta P}{L} \right)^{\frac{1}{n}} \quad [22]$$

where λr_m is the effective tube radius for the flow of a power-law fluid, defined by

$$\lambda r_m = \left[\frac{(3 + \frac{1}{n}) (2K)^{\frac{1}{n}} G_m}{\pi} \right]^{\frac{n}{3n+1}} \quad [23]$$

Inserting eq. [15] into [22] and rearranging the resulting equation, we obtain

$$u^n = \frac{(8k)^{\frac{n+1}{2}} \phi^{\frac{n-1}{2}} \lambda^{3n+1}}{\left[(3 + \frac{1}{n})^n \epsilon^{n-1} (2K) \right]} \left(\frac{\Delta P}{L} \right) \quad [24]$$

The apparent viscosity in the network can then be written, according to the definition [2],

$$\mu_{app} = \frac{K}{\lambda^{3n+1}} \left(\frac{3n+1}{4n} \right)^n \left(\frac{\sqrt{2} \epsilon u}{\sqrt{k \phi}} \right)^{n-1} \quad [25]$$

From eq. [25], we can also obtain the apparent shear rate in the network (see Appendix A). The resulting expression is similar to eq. [5], with the following "constant" or coefficient:

$$C = \sqrt{2} \epsilon \lambda^{\frac{3n+1}{1-n}} \quad [26]$$

We can thus express, even for the random networks, the dependency of the apparent viscosity (or the apparent shear rate) on the Darcy velocity and permeability in the same manner as that of eq. [5] from the capillary bundle model. It is noted, however, that the parameters, ϵ and λ , also depend on the permeability because they are implicit functions of the network structure. The effect of these parameters on the apparent shear rate is examined below.

In order to bring the value of eq. [26] to the experimentally measured value $C = 6.0$ of eq. [5], making $\lambda > 1$ will have the largest impact. The physical significance of the above observation is this: due to its shear-thinning nature, the effective radius λr_m for the flow of a power-law fluid is always larger than the effective radius r_m for the flow of a Newtonian fluid, when the connectivity and the variable cross-section of flow channels are taken into consideration. In the capillary bundle model, the two radii are implicitly assumed to be identical.

III.3. NETWORKS WITH BIMODAL DISTRIBUTION OF TUBE RADII

In order to see how the connectivity of flow channels and their variable cross-section affect the apparent viscosity of a power-law fluid, we will consider, for simplicity, a network with a bimodal probability distribution of tube radii (or pore sizes). That is, expressed in normalized form, θ fraction of the tubes will have a radius of unity and the remaining $(1-\theta)$ fraction will have a radius of α , which are distributed randomly in the network:

$$p(r) = \theta \delta(r-1) + (1-\theta) \delta(r-\alpha) \quad [27]$$

To obtain the effective radius r_m for Newtonian fluids, we insert eqs. [11] and [27] into [9]:

$$\frac{\theta}{1 + (\frac{z}{2} - 1) r_m^4} + \frac{(1-\theta)}{\alpha^4 + (\frac{z}{2} - 1) r_m^4} = \frac{1}{\frac{z}{2} r_m^4}$$

which can be solved for r_m as a function of θ , α and z as follows

$$r_m^4 = \left[B + \sqrt{B^2 + 2\alpha^4(z-2)} \right] / (z-2) \quad [28]$$

where

$$B = \frac{z\theta}{2} (1 - \alpha^4) + (\frac{z}{2} - 1)\alpha^4 - 1.$$

To obtain the effective radius λr_m for power-law fluids, we insert eqs. [17] and [27] into [20]:

$$\frac{\theta}{\left[1 + \left(\frac{z}{2} - 1\right)(\lambda r_m)^{3+\frac{1}{n}}\right]^n} + \frac{(1-\theta)}{\left[\alpha^{3+\frac{1}{n}} + \left(\frac{z}{2} - 1\right)(\lambda r_m)^{3+\frac{1}{n}}\right]^n} = \frac{1}{\left[\frac{z}{2}(\lambda r_m)^{3+\frac{1}{n}}\right]^n} \quad [29]$$

which can be solved for λr_m as a function of θ , α , n and z . As the above equation is implicit in λr_m , it needs to be solved numerically. The radius ratio, λ , can thus be obtained from eqs. [28] and [29].

To obtain ϵ , we calculate a from eqs. [14] and [27]:

$$a^2 = \int_0^\infty r^2 p(r) dr = \theta + (1-\theta)\alpha^2. \quad [30]$$

Inserting the parameters λ and ϵ calculated from the above equations into eq. [25], we can now study how the apparent viscosity is affected by the structure of the network. Before we consider the general case, two simpler cases will be studied first, in order to obtain a better understanding of the model. The first is the case of $z = 2$, i.e., the network is a bundle of unconnected capillary tubes, but with a series of constrictions and expansions (Fig. 12(a)). The second case is when $\alpha = 0$, i.e., the network consists of capillary tubes of a uniform radius, but a certain fraction of the connections are blocked randomly (Fig. 12(b)).

III.3.1. CAPILLARY TUBES WITH A SERIES OF CONSTRICTIONS AND EXPANSIONS

In order to circumvent the inadequacy of the capillary bundle model, a number of researchers^{1,19,21} adopted, as a model of a porous medium, capillary tubes with a series of constrictions and expansions. Such a model can be considered within the framework of the present theory simply by setting $z = 2$. In Appendix C, the apparent shear rate expression for this simplified case is derived as eq. [C3]. It is noted that eq. [C3] is in fact identical to the one derived by Teeuw and Hesselink¹, as eq. [13] of their paper. Their derivation was, however, limited to this particular case, and was made in a deterministic way, i.e., the constrictions and expansions were placed regularly, rather than randomly as we do.

Fig. 13 shows the coefficient C from the apparent shear rate of [C3] as a function of the radius ratio of narrow to wide tube segments (α) and the fraction of wider tube segments (θ), when $n = 0.5$. The C value from our experiments (6.0) is also shown for comparison. We see that the constrictions and expansions could indeed increase the coefficient value from what is obtainable from the capillary bundle model. The increase in coefficient is more pronounced when the fraction of the wider tube segments is larger than the fraction of the narrower tube segments ($\theta > 0.5$).

III.3.2. A RANDOM NETWORK OF OPEN AND CLOSED CHANNELS

We now study how the connectivity of flow channels affects the apparent viscosity, by setting $\alpha = 0$. That is, θ fraction of the tubes will have a radius of unity and the remaining $(1-\theta)$ fraction will have a zero radius, forming a random network of open and closed channels. The porous body created thus has a uniform tube radius, but the tubes are randomly connected and tortuous. In Appendix D, the derivation of the apparent viscosity expression for this case is given.

Fig. 14(a) shows the coefficient C of the apparent shear rate as a function of the open channel fraction, θ , and the power-law exponent, n , when the coordination number, $z = 6$. The value of $C = 6.0$ from eq. [5], which fits experimental data well, is also shown. We see that the coefficient value again becomes larger than what is obtainable from the capillary bundle model. As the fraction of the open channel decreases, i.e., the flow path becomes more tortuous, the increase in coefficient becomes more pronounced. Fig. 14(b) is similar to Fig. 14(a), except that the coordination number is now $z = 4$. Interestingly, we find that the C value from the experiments (6.0) can be obtained when the effective coordination number, θz , is about 2.3 to 2.5. This point will be further elaborated below.

III.3.3. GENERAL CASE OF BIMODAL DISTRIBUTION OF TUBE RADII

In the above two subsections, we examined the effects of the variable cross-section of flow channels and the connectivity of flow channels on the apparent shear rate, by considering two limiting cases of the bimodal distribution. The general case of bimodal distribution of tube radii will be studied here by solving eqs. [28] and [29], and inserting the resulting values of λ and ϵ into [26].

Fig. 15(a) shows the coefficient C of the apparent shear rate as a function of the fraction of wider tube, θ , and the radius ratio, α , when the coordination number, $z = 4$, and the power-law exponent, $n = 0.5$. Figs. 15(b) and (c) are similar to Fig. 15(a) except that $z = 6$ and 8 , respectively. We see that when the radius ratio (α) is small, the coefficient value is almost independent of α , which means that there will be practically no flow through the thinner tubes due to the shear-thinning nature of the polymer solution. This is an interesting observation because, even when a polymer molecule is accessible to a narrow pore channel, there will be practically no movement of polymer through the channel. When α is smaller than about 0.2, therefore, the network behaves similar to the simpler network of open and closed channels considered in the above section. As we have noted in the above section, the experimentally reasonable value of the coefficient ($C = 6.0$) can again be obtained with the effective coordination number, θz , of about 2.4.

Fig. 16 is similar to Fig. 15(b) except that $n = 0.4$ instead of 0.5. We see that the power-law exponent does not affect the coefficient as significantly as the parameters which represent the pore structure, i.e., θ , α and z .

III.4. DISCUSSION

From the above study, the following three observations can be made. First, the fact that the effective coordination number, θz , of about 2.3 to 2.5 fits experimental data well suggests that the bulk of polymer flow occurs almost without any branching of the flow channels, even though the paths may be tortuous. Second, the bulk of polymer flow also occurs through the wider channels of the porous body, and the flow through the narrower channels is negligible. Third, comparison of the results from the two limiting cases suggests that the connectivity of flow channels is more important than the constrictions and expansions of the channels, in explaining the experimental observation of $C = 6.0$.

From the above observations, we may conclude that, to the polymer flow, the detailed structure of the small-scale pore channels is immaterial and only the connectivity of the wider channels is important. Polymer solutions generally zip through the wide channels of porous media, largely ignoring the small-scale pore channels of the porous body. In a tortuous and interconnected geometry of porous media, a shear-thinning fluid can flow much more effectively, through those flow paths which are wider, than a Newtonian fluid. This recognition can explain why the experimentally measured value of C in eq. [5] is much higher than the prediction from the capillary bundle model; and why eq. [5] seems to apply for a wide variety of porous media.

Experimental evidence^{3,6} and theoretical considerations^{22,23} show that when a polymer solution flows in a thin capillary tube, the polymer molecules are excluded from the vicinity of the tube wall, due to the configurational restrictions imposed on the polymer chains by the wall. When a polymer solution flows in a porous medium, therefore, it is expected that a polymer-free, water layer will exist near the pore walls and, consequently, the apparent viscosity in the porous body will be lower than that for a bulk solution. The simple consideration given in Appendix E suggests that the inadequacy of the capillary bundle model for the shear-thinning fluid is due more to its failure to account for the connectivity of flow channels, as described in the above, than to its failure to account for the polymer exclusion near the pore walls.

While the effective medium theory proved to be useful in understanding the effects of the connectivity of flow channels and their variable cross-section in a simple manner, its shortcoming due to its approximate nature should be noted here. The prediction from the effective medium theory is known to be poor near the percolation threshold¹⁸, at which continuous flow channels cease to exist. Use of the theory developed here should therefore be avoided near the percolation threshold. For example, the percolation threshold for the random network of open and closed channels (Section III.3) can be calculated from eq. [D4] of Appendix D, by setting $\lambda r_m = 0$:

$$\theta = 1 - \left(\frac{z - 2}{z} \right)^n \quad [31]$$

We see that the fraction of open channels at the percolation threshold depends not only on the coordination number z , but also on the power-law exponent n . In reality, it should be independent of n . This

shortcoming arises from the averaging process involving the exponent in eq. [20]. For almost all porous media for which the apparent viscosity is considered, however, the network structure will be sufficiently removed from the percolation threshold, and the effective medium theory should be valid.

In this study, for simplicity, the pore structure was limited to the bimodal distribution of pore sizes, even though the theoretical derivation of Section III.2 can be applied more generally. Investigation with a more realistic distribution of pore sizes to explain the experimental observations in a more quantitative manner is warranted.

IV. CONCLUSIONS

1. An apparent shear rate equation has been developed to relate the flow behavior of xanthan solutions in cores having different permeabilities, lithologies, and oil saturations. The equation can also be used to relate the apparent shear rates in porous media to those of the viscometer. Although the shear rate dependence on flow velocity and effective permeability agrees with that predicted by traditional capillary bundle model approaches, the value of the experimentally-determined constant coefficient is higher than those predicted by the models.
2. Although Newtonian behavior was obtained at low shear rates in the viscometer, power-law behavior was obtained in porous media at 25°C for polymer concentrations above the overlap concentration C^* . Newtonian behavior was exhibited at low shear rates in porous media for polymer concentrations near C^* at 25°C and above C^* at 80°C. Two equations have been developed to predict these two different flow behaviors in porous media a priori from viscometer data.
3. The apparent viscosity expression obtained from a network model with a bimodal distribution of tube radii fits the experimental data well when the effective coordination number, θz , is about 2.3 to 2.5. This suggests that most of the polymer flow occurs almost without any branching of the flow channels, even though the paths may be tortuous.
4. The bimodal network model also shows that when the radii ratio of narrow to wide tubes is 0.2 or smaller, polymer flow occurs mainly through the wider channels of the porous body, and the flow through the narrower channels is negligible.
5. Since polymer solutions generally flow mainly through the wide channels of porous media, and largely bypass small-scale pore channels of the porous body, the detailed structure of the small-scale pore channels is almost immaterial to the polymer flow, and only the connectivity of the wider channels is important. This may explain why eq. [5] applies for a wide variety of porous media.
6. The inadequacy of the capillary bundle model for the shear-thinning fluid is due more to its failure to account for the connectivity of wide flow channels than to its failure to account for the polymer exclusion near the pore walls. Depletion layer effects reported by other

investigators experimentally were not observed in our study.

NOMENCLATURE

a	= average tube radius defined by eq. [14]
C	= constant in eqs. [1], [5]; the coefficient defined by eq. [26]
C_p	= polymer concentration, ppm
C^*	= overlap concentration for polymer solution, ppm
g, g_m	= flow conductivity for a Newtonian fluid, defined by eq. [11]; effective flow conductivity
G, G_m	= flow conductivity for a power-law fluid, defined by eq. [17]; effective flow conductivity
k, k_{aq}	= permeability; aqueous-phase permeability, cm^2
K	= consistency index defined by eq. [4], $cp \text{ sec}^{-1}$
n	= power-law exponent defined by eq. [4]
p	= probability distribution of tube radii
q	= flux defined by eqs. [10] and [16], cm^3/sec
r, r_m	= tube radius; effective tube radius for a Newtonian fluid, cm
S_{aq}	= aqueous-phase saturation
u	= Darcy velocity, cm/sec
z	= coordination number for network
$\Delta P/L$	= pressure gradient, gr/cm^3

Greek

α	= radius ratio, in eq. [27]
ξ	= $1 - \delta/R$, defined in eq. [E4]
ϵ	= a/r_m
$\dot{\gamma}_{app}$	= apparent shear rate defined by eq. [A3]
$\dot{\gamma}_{eff}$	= "effective" shear rate, sec^{-1}
λ	= ratio of effective radius for flow of a power-law fluid to a Newtonian fluid
μ	= viscosity from viscometer, cp
μ_{app}	= apparent viscosity in porous media, cp
μ_0, μ_∞	= Newtonian viscosity at zero and infinite shear rates, cp
μ_w	= water viscosity, cp
ϕ	= porosity
θ	= fraction of tubes with a radius of unity, in eq. [27]

ACKNOWLEDGMENTS

We would like to acknowledge the efforts of J. C. Roffall and J. K. McCarthy to obtain the experimental data and the discussions with G. F. Teletzke.

REFERENCES

1. Teeuw, D., and Hesselink, F.T., "Power-Law Flow and Hydrodynamic Behavior of Biopolymer Solutions in Porous Media", Paper SPE 8982 presented at SPE 5th Intern. Symp. Oilfield Geotherm. Chem., Stanford, CA, May 28-30, 1980.
2. Willhite, G.P., and Uhl, J.T., "Correlation of the Mobility of Biopolymer with Polymer Concentration and Rock Properties in Sandstone", *Polym. Mater. Sci. Eng.* **55**, 577-581 (1986).
3. Chauveteau, G., "Fundamental Criteria in Polymer Flow Through Porous Media," in "Water Soluble Polymers", *Adv. Chem. Ser.* **213**, J. E. Glass ed., 227-267 (1984).
4. Savins, J. G., "Non-Newtonian Flow Through Porous Media," *Ind. Eng. Chem.* **61**, 18-47 (1969).
5. Hejri, S., Willhite, G.P., and Green D.W., "Development of Correlations to Predict Flocon 4800 Biopolymer Mobility in Porous Media", Paper SPE/DOE 17396 presented at SPE/DOE 6th Symp. Enhanced Oil Recovery, Tulsa, OK, April 17-20, 1988.
6. Chauveteau, G., and Zaitoun, A., "Basic Rheological Behavior of Xanthan Polysaccharide Solutions in Porous Media: Effects of Pore size and Polymer Concentration", *Proc. European Symp. Enhanced Oil Recovery*, F. J. Fayers, ed., 197-212 (1981).
7. Chauveteau, G., and Kohler, N., "Influence of Microgels in Xanthan Polysaccharide Solutions on Their Flow Through Various Porous Media", Paper SPE 9295 presented at SPE 55th Annual Tech. Conf., Dallas, TX, Sept. 21-24, 1980.
8. Kolodziej, E.J., "Mechanism of Microgel Formation in Xanthan Biopolymer Solutions", Paper SPE 16730 presented at SPE 62nd Annual Tech. Conf., Dallas, TX, Sept. 27-30, 1987.
9. Kohler, N., and Chauveteau, G., "Xanthan Polysaccharide Plugging Behavior in Porous Media--Preferential Use of Fermentation Broth", *J. Pet. Tech.* (Feb. 1981), 349-358.
10. Holzwarth, G., "Conformation of the Extracellular Polysaccharide of Xanthomonas Campestris" *Biochemistry* **15**, 4333-4339 (1976).
11. Gogarty, W. B., Levy, G. L., and Fox, V. G., "Viscoelastic Effects in Polymer Flow Through Porous Media," SPE Paper 4025 presented at SPE 47th Annual Fall Meeting, San Antonio, TX, Oct. 8-11, 1972.
12. Holzwarth, G., "Molecular Weight of Xanthan Polysaccharide," *Carbohydrate Research* **66**, 173 (1978).
13. Christopher, R. H., and Middleman, S., "Power-Law Flow Through a Packed Tube," *Ind. Eng. Chem. Fund.* **4**, 422-426 (1965).
14. Bird, R. B., Stewart, W. E., and Lightfoot, E. N., *Transport Phenomena* John Wiley & Sons, N.Y. (1960), 197-207.
15. Koplik, J., "Creeping Flow in Two-Dimensional Networks", *J. Fluid Mech.* **119**, 219-247 (1982).
16. Levine, S., and Cuthiell, D. L., "Relative Permeabilities in Two-Phase Flow through Porous Media: An Application of Effective Medium Theory", *J. Canadian Petrol. Tech.* **25**, 74-84 (1986).
17. Kirkpatrick, S., "Percolation and Conduction", *Rev. Mod. Phys.*, **45**, 574-588 (1973).
18. Koplik, J., "On the effective medium theory of random linear networks", *J. Phys. C.*, **14**, 4821-4837 (1981).
19. Duda, J. L., Hong, S. A., and Klaus, E. E., "Flow of Polymer Solutions in Porous Media:

Inadequacy of the Capillary Model", Ind. Eng. Chem. Fund., 22, 299-305 (1983).

20. Larson, R. G., "Derivation of Generalized Darcy Equations for Creeping Flow in Porous Media", Ind. Eng. Chem. Fund., 20, 132-137 (1981).
21. Sheffield, R. E., and Metzner, A. B., "Flows of Nonlinear Fluids through Porous Media," Amer. Inst. Chem. Eng. J. 22, 736-744 (1976).
22. Aubert, J. H., and Tirrell, M., "Effective Viscosity of Dilute Polymer Solutions near Confining Boundaries", J. Chem. Phys. 77, 553-561 (1982).
23. Park, O. O., and Fuller, G. G., "Dynamics of Rigid and Flexible Polymer Chains in Confined Geometries. Part I: Steady Simple Shear Flow", J. Non-Newtonian Fluid Mech. 15, 309-329 (1984).
24. Milas, M., and Rinaudo, M., "Conformational Investigation on the Bacterial Polysaccharide Xanthan", Carbohydrate Res. 76, 189-196 (1979).
25. Bird, R. B., Armstrong, R. C., and Hassager, O., Dynamics of Polymeric Liquids, Vol. 1, John Wiley, New York, 171-173 (1987).

APPENDIX A: Shear Rate Expressions in Porous Media

Capillary bundle model approaches^{1,4,13,14} predict that the apparent viscosity of a power-law fluid in porous media is related to the Darcy velocity u by the following equation:

$$\mu_{app} = K \left[\frac{3n+1}{4n} \right]^n \left[\frac{Cu}{\sqrt{k\phi}} \right]^{n-1} \quad [A1]$$

In this equation, the values of the consistency index K and the power-law exponent n are determined from viscometer measurements. The theoretical value of C depends on the approach taken and the values used to account for the tortuosity of the porous medium. Values of C from several different approaches are summarized in Table II. All of these values are much lower than the value of $C = 6.0$ which we obtained from our experiments.

In correlating the apparent viscosity data, Christopher and Middleman¹³ and others defined the "effective" shear rate in porous media, which is given by eq. [1] of the Introduction. Inserting eq. [1] into [A1], we obtain

$$\mu_{app} = \left[\frac{3n+1}{4n} \right]^n K \dot{\gamma}_{eff}^{n-1} \quad [A2]$$

To make eq. [A2] conform with the power-law equation [4], the definition of the "effective" shear rate necessitates additionally defining the "effective" consistency index in porous media, $\left(\frac{3n+1}{4n} \right) K$.

In this study, a simpler approach is taken by defining the "apparent" shear rate by way of the power-law equation:

$$\dot{\gamma}_{app} = \left[\frac{\mu_{app}}{K} \right]^{\frac{1}{n-1}} \quad [A3]$$

By inserting eq. [A1] into [A3], we obtain

$$\dot{\gamma}_{app} = C \left[\frac{3n+1}{4n} \right]^{\frac{n}{n-1}} \frac{u}{\sqrt{k\phi}} \quad [A4]$$

which is employed as eq. [5] in Section II. The above expression is also employed for eq. [26], even though C in the equation is now not a constant, but a function of the network parameters.

APPENDIX B: Derivation of Eq. [18] by the Effective Medium Theory

Consider a tube in the network, through which a power-law fluid flows according to the relation [16], and whose flow conductivity is G , as defined by eq. [17]. When the effective conductivity of the network is G_m and the average pressure gradient is $(\Delta P/L)_m$, we would like to obtain the pressure gradient for the tube. Let G_e be the conductivity due to the flow between the nodes at the entrance and the exit of the tube, but not through the tube.

The flow through the node at the entrance (or the exit) of the tube is, approximately,

$$\left(\frac{z}{2} \right) q = \frac{z}{2} G_m \left(\frac{\Delta P}{L} \right)_m^{\frac{1}{n}} \quad [B1]$$

If the conductivity of every tube in the network were G_m , we should have, from eq. [B1],

$$\frac{z}{2} G_m \left(\frac{\Delta P}{L} \right)_m^{\frac{1}{n}} = (G_m + G_e) \left(\frac{\Delta P}{L} \right)_m^{\frac{1}{n}} \quad [B2]$$

from which we can obtain

$$G_e = \left(\frac{z}{2} - 1 \right) G_m \quad [B3]$$

When the conductivity of the tube is G and the pressure gradient is $(\Delta P/L)$, we now obtain, instead of eq. [B2],

$$\frac{z}{2} G_m \left(\frac{\Delta P}{L} \right)_m^{\frac{1}{n}} = (G + G_e) \left(\frac{\Delta P}{L} \right)^{\frac{1}{n}} \quad [B4]$$

Inserting eq. [B3] into [B4] and rearranging, we obtain

$$\left(\frac{\Delta P}{L} \right) = \left[\frac{\frac{z}{2} G_m}{G + \left(\frac{z}{2} - 1 \right) G_m} \right]^n \left(\frac{\Delta P}{L} \right)_m \quad [B5]$$

APPENDIX C: Apparent Viscosity for Capillary Tubes with a Series of Constrictions and Expansions

When $z = 2$, r_m and λr_m can be obtained from eqs. [28] and [29], respectively,

$$r_m = [\theta + (1 - \theta)/\alpha^4]^{-\frac{1}{4}} \quad [C1]$$

$$\lambda r_m = [\theta + (1 - \theta)/\alpha^{3n+1}]^{-1/(3n+1)} \quad [C2]$$

Inserting eqs. [C1], [C2] and [30] into eq. [26], we can obtain the apparent shear rate for capillary tubes with a series of constrictions and expansions:

$$\dot{\gamma}_{app} = \sqrt{\theta + (1 - \theta)\alpha^2} \left[\frac{\frac{n+1}{8^{\frac{1}{2}}} (\theta + (1 - \theta)/\alpha^4)^{\frac{n+1}{2}}}{2 \left(3 + \frac{1}{n}\right)^n (\theta + (1 - \theta)/\alpha^{3n+1})} \right]^{\frac{1}{1-n}} \frac{u}{\sqrt{k\phi}} \quad [C3]$$

The physical significance of the effective medium theory can be better understood by re-deriving λr_m of eq. [C2], as Teeuw and Hesselink¹ did, in a deterministic manner. For tube segments of a unit radius and of radius, α , we can obtain from eq. [16] the respective pressure gradient:

$$(\Delta P/L)_1 = \left[\left(\frac{1}{\frac{3+n}{\pi}} \right) (2K)^{\frac{1}{n}} q \right]^n \quad [C4]$$

$$(\Delta P/L)_\alpha = \left[\frac{(3+1/n)(2K)^{\frac{1}{n}} q}{\pi \alpha^{3+\frac{1}{n}}} \right]^n \quad [C5]$$

for both of which the flow rate is identical. The average pressure gradient can be calculated in terms of the relative fractions of the tube segments:

$$\left(\frac{\Delta P}{L} \right)_m = \theta \left(\frac{\Delta P}{L} \right)_1 + (1 - \theta) \left(\frac{\Delta P}{L} \right)_\alpha = \left[\theta + \frac{(1 - \theta)}{\alpha^{3n+1}} \right] \left[\frac{3+1/n}{\pi} (2K)^{\frac{1}{n}} q \right]^n \quad [C6]$$

The effective tube radius, λr_m , will then be

$$\frac{1}{(\lambda r_m)^{3n+1}} = \theta + \frac{(1 - \theta)}{\alpha^{3n+1}} \quad [C7]$$

which is in fact eq. [C2], as derived alternately by the effective medium theory. Eq. [C6] thus illustrates how the pressure fluctuation in the network is averaged in the effective medium theory, which is carried out by eq. [20].

APPENDIX D: Apparent Viscosity for a Random Network of Open and Closed Channels

For a Newtonian fluid, inserting eqs. [27] and [11] into [9], we obtain

$$\theta \left[\frac{r_m^4 - 1}{2 + (z - 2)r_m^4} \right] + \frac{(1 - \theta)}{(z - 2)} - 0 \quad [D1]$$

which can be solved for r_m as

$$r_m = \left[\frac{\theta z - 2}{z - 2} \right]^{\frac{1}{4}} \quad [D2]$$

For the power-law fluid, inserting eqs. [27] and [17] into [20], we obtain

$$\theta \left[\frac{z(\lambda r_m)^{3+\frac{1}{n}}}{2 + (z-2)(\lambda r_m)^{3+\frac{1}{n}}} \right]^n + (1 - \theta) \left(\frac{z}{z-2} \right)^n - 1 = 0 \quad [D3]$$

which can be solved for λr_m as

$$\lambda r_m = \left[\frac{2A}{z - (z - 2)A} \right]^{\frac{n}{3n+1}} \quad [D4]$$

where

$$A = \left[\frac{1}{\theta} - \left(\frac{1 - \theta}{\theta} \right) \left(\frac{z}{z - 2} \right)^n \right]^{\frac{1}{n}}$$

The radius ratio, λ , can now be obtained from eqs. [D2] and [D4] as a function of θ , z and n . From eq. [14], we can obtain

$$a = \sqrt{\theta} \quad [D5]$$

The apparent shear rate for a random network of open and closed channels can be subsequently calculated by inserting eqs. [D2], [D4] and [D5] into eq. [26].

APPENDIX E: Flow of a Power-Law Fluid with a Polymer-Free Layer at the Pore Wall in the Capillary Bundle Model

In order to see if polymer exclusion near the pore wall is indeed mainly responsible for the inadequate prediction of apparent viscosity by the capillary bundle model, in this appendix, the capillary bundle model for the flow of a power-law fluid in a porous medium is modified to account for the presence of a polymer-free water layer at the pore walls. As suggested by Chauveteau and Zaitoun⁶, it is assumed that the thickness δ of the layer is approximately half the length of a polymer molecule and thus is constant.

Consider a circular tube with a characteristic radius of R , in which a power-law fluid flows in the central area of $r = 0$ to $R - \delta$, and a polymer-free water flows in the remaining annular area near the wall. The flow rate from the tube can be calculated as

$$q = \left[\frac{\pi(R - \delta)^{3+\frac{1}{n}}}{\left(3+\frac{1}{n}\right)(2K)^{\frac{1}{n}}} \right] \left(\frac{\Delta P}{L} \right)^{\frac{1}{n}} + \left[\frac{\pi(R^4 - (R - \delta)^4)}{8\mu_w} \right] \left(\frac{\Delta P}{L} \right) \quad [E1]$$

The Darcy velocity for the capillary bundle model will be

$$u = \frac{\phi q}{\pi R^2} \quad [E2]$$

According to the capillary bundle model, the characteristic radius can be replaced with the permeability by the relation

$$R = \sqrt{8k/\phi} \quad [E3]$$

Inserting eq. [E3] and the definition of the apparent viscosity [2] into [E2], we obtain

$$\left[\frac{8^{\frac{n+1}{2n}} \xi^{\frac{3+1}{n}} \left(\frac{u^2}{k\phi} \right)^{\frac{1-n}{2n}}}{\left(3+\frac{1}{n}\right)} \right] \left(\frac{\mu_{app}}{2K} \right)^{\frac{1}{n}} + (1 - \xi^4) \left(\frac{\mu_{app}}{\mu_w} \right) = 1 \quad [E4]$$

where $\xi = 1 - \delta/R$. The apparent viscosity is thus given by the above equation in an implicit form. We note that when $\xi = 0$, i.e., $\delta = R$, the apparent viscosity becomes water viscosity; and when $\xi = 1$, i.e., $\delta = 0$, the equation becomes

$$\mu_{app} = K \left(\frac{3n+1}{4n} \right)^n \left(\frac{\sqrt{2} u}{\sqrt{k\phi}} \right)^{n-1} \quad [E5]$$

for the power-law fluid alone. The above equation can be obtained from eq. [25] by setting $\epsilon = 1$ and $\lambda = 1$; that is, all the tubes in the network have the same radius and are not connected, as in the capillary bundle model (see Appendix A).

When the Darcy velocity becomes large, the above equation approaches the following equation

$$\mu_{app} = \frac{K}{\xi^{3n+1}} \left(\frac{3n+1}{4n} \right)^n \left(\frac{\sqrt{2}u}{\sqrt{k\phi}} \right)^{n-1} \quad [E6]$$

which is similar to eq. [E5]: however, the term ξ representing the polymer-free layer makes the prediction of the apparent viscosity from eq. [E6] even higher than that from eq. [E5]. When the Darcy velocity becomes small, eq. [E4] approaches

$$\mu_{app} = \frac{\mu_w}{1 - \xi^4} \quad [E7]$$

The physical significance of the above equation is that when the Darcy velocity is small, a very viscous (almost rigid) slug of the polymer solution glides on a layer of water, so that the apparent viscosity is governed only by the relative thickness of the water layer and water viscosity. Both of the above limiting behaviors are not what are observed experimentally. Therefore, while polymer exclusion near the pore wall may be partly responsible for the lower apparent viscosity measured, it does not appear to be the major contributor.

Table I

VISCOMETER PARAMETERS

Cp (ppm)	n	K (cp sec ⁿ⁻¹)	μ_0 (cp)
300	0.75	17	8.6
600	0.60	43	26.0
1200	0.48	195	102.0
1600	0.35	620	1000.0

Table II

VALUES OF COEFFICIENT C IN SHEAR RATE EQUATION

Source	C
Present study	6.0
Teeuw and Hesselink ¹	$\sqrt{2} = 1.414$
Christopher and Middleman ¹³	$\sqrt{2} / \sqrt{\frac{25}{12}} = 0.980$
Bird, et al. ¹⁴	$\sqrt{2} \cdot \sqrt{\frac{25}{12}} = 2.041$

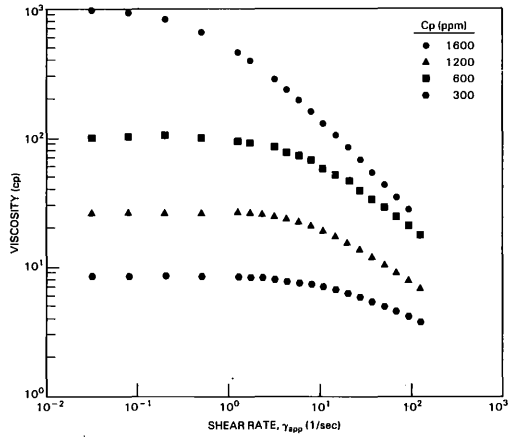


Fig. 1—Viscometer rheology of xanthan solutions at 25°C.

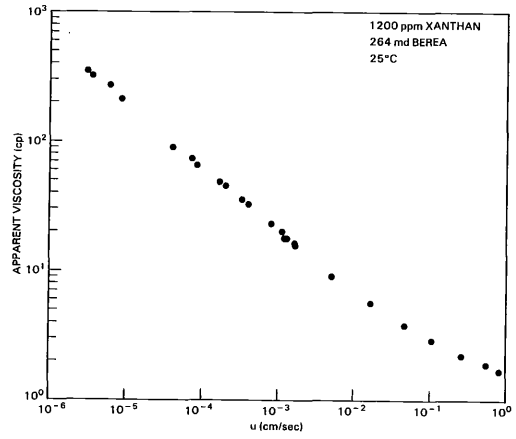


Fig. 2—Flow behavior of 1,200 ppm xanthan in 264 md Berea sandstone.

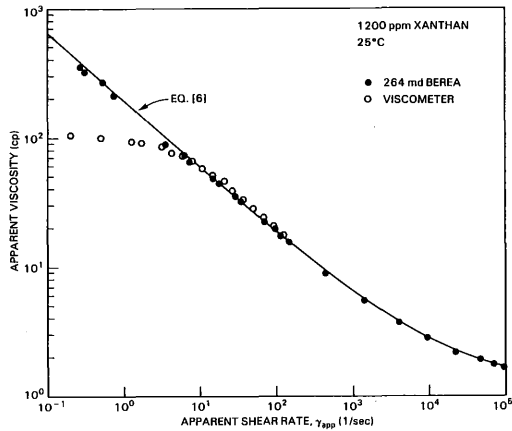


Fig. 3—Comparison of 1,200 ppm xanthan rheology in 264 md Berea sandstone and viscometer at 25°C.

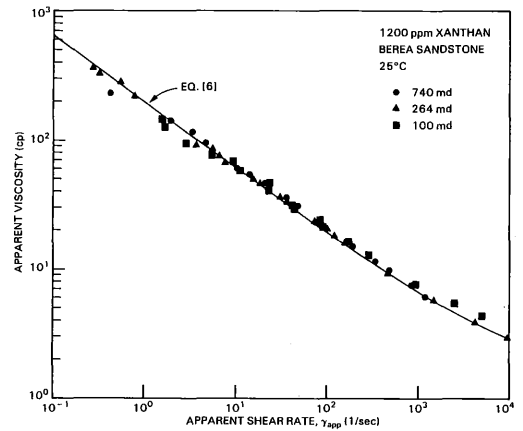


Fig. 4—Influence of Berea sandstone permeability on flow behavior of 1,200 ppm xanthan at 25°C.

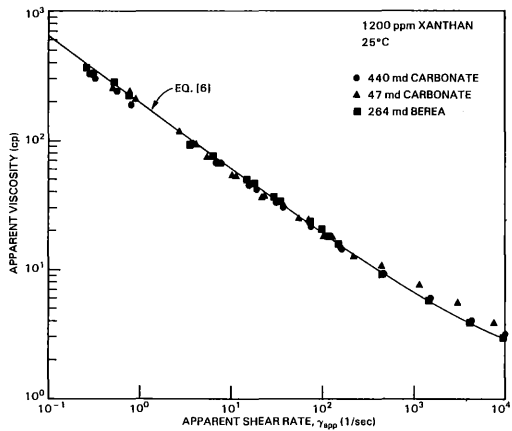


Fig. 5—Influence of lithology on flow behavior of 1,200 ppm xanthan at 25°C.

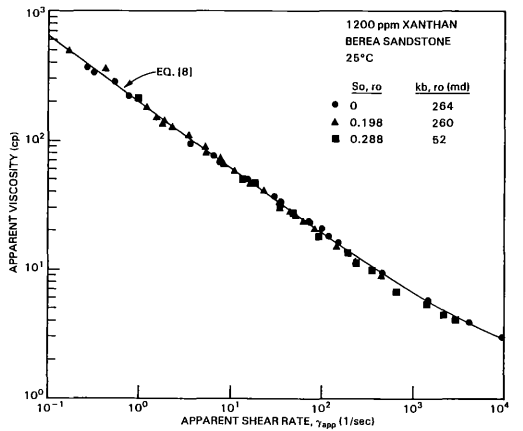


Fig. 6—Influence of residual oil saturation on flow behavior of 1,200 ppm xanthan in Berea sandstone at 25°C.

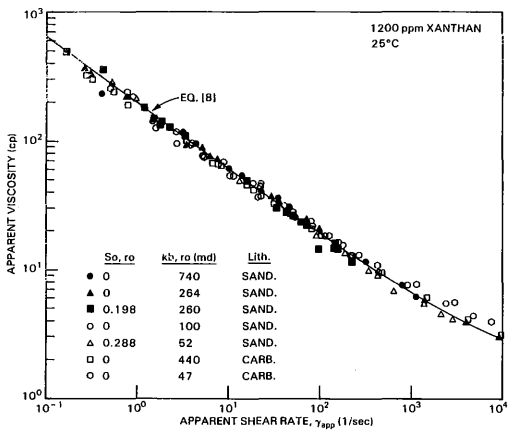


Fig. 7—Summary of flow behavior of 1,200 ppm xanthan in porous media at 25°C.

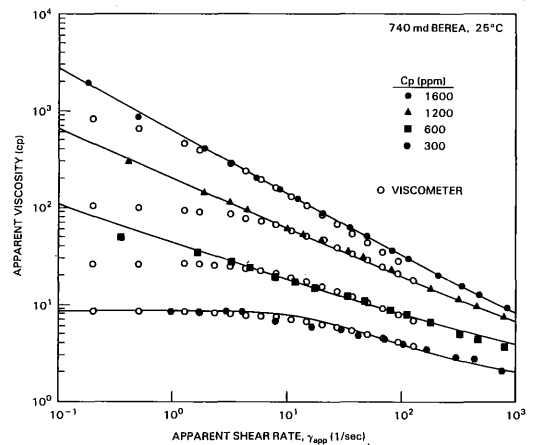


Fig. 8—Comparison of porous media and viscometer rheologies for various xanthan concentrations at 25°C.

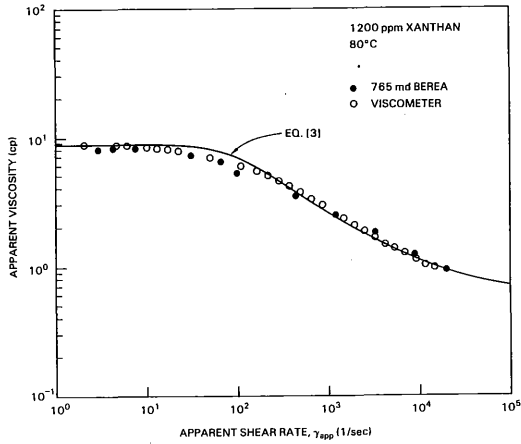


Fig. 9—Comparison of 1,200 ppm xanthan rheology in 765 md Berea sandstone and viscometer at 80°C.

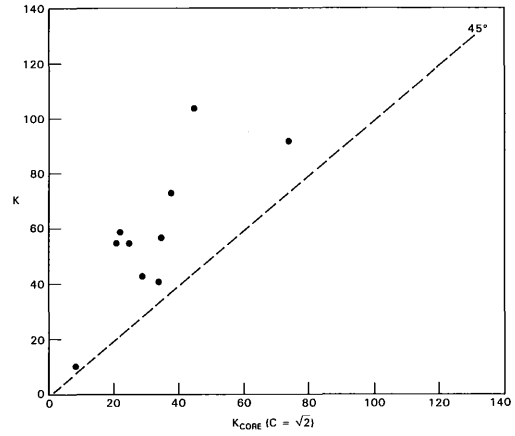


Fig. 10a—Comparison of consistency indices measured in viscometer (K) and calculated from porous media results with $C=\sqrt{2}$ ($K_{core}, C=\sqrt{2}$) by Teeuw and Hesselink (Ref. 1).

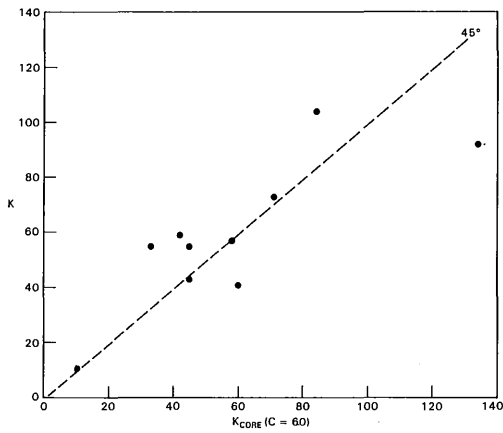


Fig. 10b—Comparison of consistency indices measured in viscometer (K) and calculated from Teeuw and Hesselink's porous media results using value of $C=6.0$ obtained in present study ($K_{core}, C=6.0$).

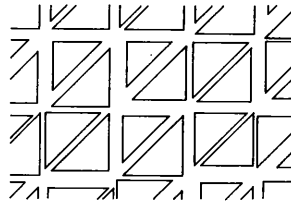


Fig. 11—Network of capillary tubes.

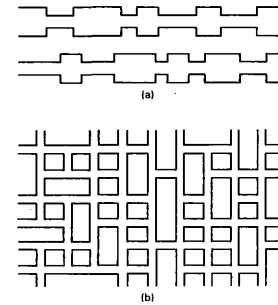


Fig. 12—(a) Capillary bundle model with a series of constrictions and expansions and (b) random network of open and closed channels.

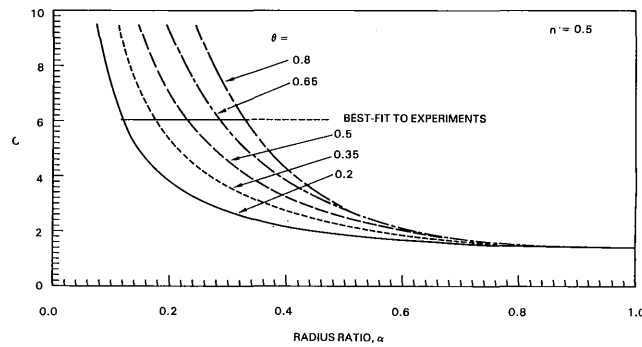


Fig. 13—The coefficient C of the apparent shear rate for the model with $z=2$ with a series of constrictions and expansions, as a function of α and θ when $n=0.5$.

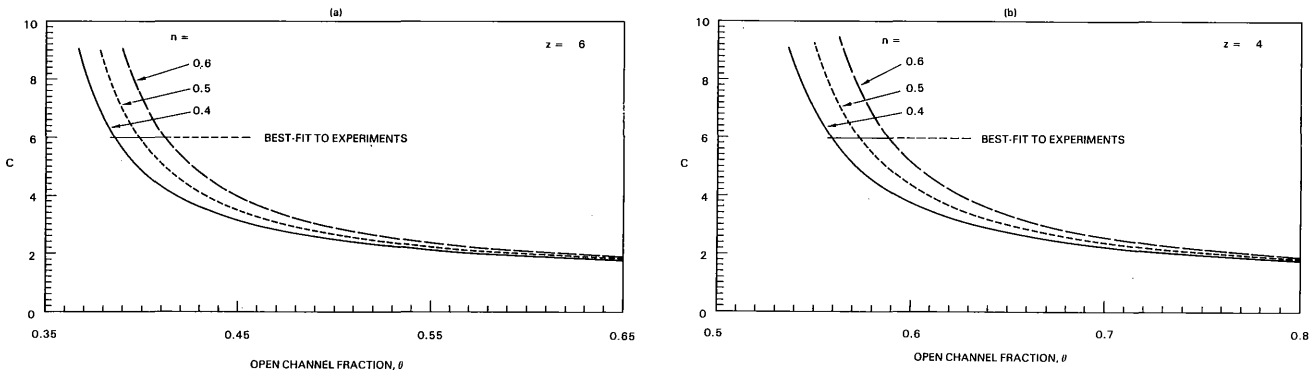


Fig. 14—The coefficient C of the apparent shear rate for the random network with open and closed channels, as a function of θ and n (a) when $z=6$; and (b) when $z=4$.

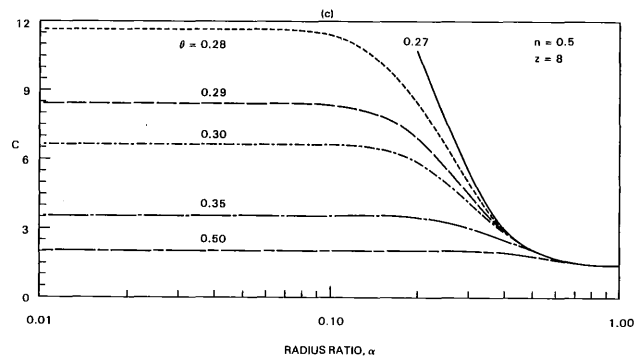
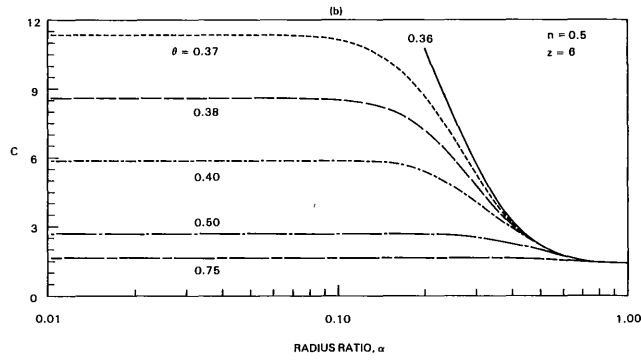
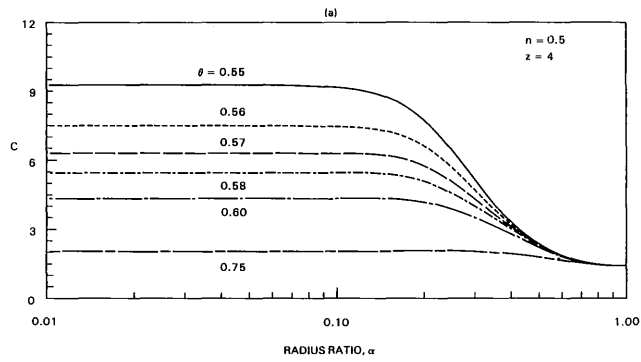


Fig. 15—The coefficient C of the apparent shear rate for the network with bimodal distribution of tube radii, as a function of α and θ when $n=0.5$ and (a) $z=4$; (b) $z=6$; and (c) $z=8$.

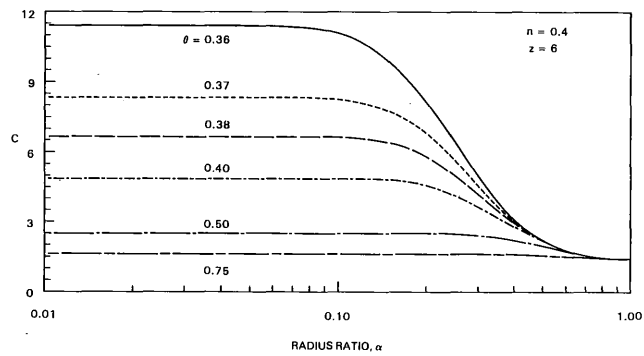


Fig. 16—The coefficient C of the apparent shear rate for the network with bimodal distribution of tube radii, as a function of α and θ when $z=6$ and $n=0.4$.